Applied Catalysis B: Environmental 158–159 (2014) 91–95

Contents lists available at ScienceDirect

Applied Catalysis B: Environmental

journal homepage: www.elsevier.com/locate/apcatb

Decoration of TiO_2 anatase nanoplates with silver nanoparticles on the {1 0 1} crystal facets and their photocatalytic behaviour

Maria-Veronica Sofianou[a], Nikos Boukos[a], Tiverios Vaimakis[b], Christos Trapalis[a,*]

[a] Institute of Advanced Materials, Physicochemical Processes, Nanotechnology and Microelectronics, National Center for Scientific Research "Demokritos", 153 10, Ag. Paraskevi, Attikis, Greece
[b] Department of Chemistry, University of Ioannina, 451 10 Ioannina, Greece

ARTICLE INFO

Article history:
Received 2 August 2013
Received in revised form 12 February 2014
Accepted 17 February 2014
Available online 24 February 2014

Keywords:
Ag/TiO_2 nanoplates
{1 0 1} {0 0 1} Facets
Photocatalysis
NO oxidation

ABSTRACT

Ag nanoparticles were photodeposited on the {1 0 1} crystal facets of the TiO_2 anatase nanoplates. This was achieved with the photoreduction of $AgNO_3$ in methanol solution in which TiO_2 anatase nanoplates were suspended while UVA irradiation was performed. The size range of the photodeposited silver nanoparticles was between 5 and 20 nm. The manipulation of their size was achieved by controlling the UVA light irradiation period of time whereas the formation on the specific facet of the TiO_2 anatase nanocrystal was managed by using methanol as a hole scavenger. The silver ions (Ag^+) were photoreduced by the electrons that were photogenerated due to the TiO_2 anatase nanoplates irradiation with UVA light. The photocatalytic activity of the nanocomposites was examined in NO oxidation, showing a higher photocatalytic activity and photonic efficiency in comparison to the pure TiO_2 anatase nanoplates.

1. Introduction

Air pollution is a great issue that plagues highly populated cities throughout the world. Nitrogen oxides (NO, NO_2) are very toxic and prominent air pollutants that plague highly populated cities causing massive health problems to the civilians such as respiratory infections, heart disease, and lung cancer but also to the environment itself for example the greenhouse effect which destroys the eco system as well as the cultural monuments of these cities [1,2].

Titanium dioxide (TiO_2) is a semiconductor that has been widely studied over the years due to its enhanced properties and has various environmental and energy applications [3–9]. The anatase phase of the TiO_2 has in most cases higher photocatalytic activity in comparison to the rutile and brookite phase. Generally, photocatalysis is based on the absorption of a photon by a photocatalyst creating electron–hole (e^-/h^+) pairs, which either recombinate or subsequently participate in redox reactions with surface radicals, like superoxide ions (O^2) and hydroxyl radicals (OH^-) [10–12]. The photocatalytic activity of the photocatalyst clearly depends on the recombination rate of the electron and hole. This implies that a low recombination rate will significantly enhance the photocatalytic properties of the photocatalyst.

Recently several studies have shown that the reduction and oxidation sites on the surfaces of the anatase TiO_2 single crystals are spatially separated. The reason for that is the selective migration of excited electrons on the {1 0 1} facets and of positive holes on the {0 0 1} facets [13,14]. Moreover, from several studies it has been reported that deposited noble metal nanoparticles trap the photogenerated electrons thereby hindering the recombination of the electron and hole pair [15,16]. There is considerable interest in the use of Ag for this purpose due to its low cost in comparison to the other noble metals [17–19].

In this study, a method for exclusively embedding Ag nanoparticles on the {1 0 1} anatase crystal facets of the nanoplates is reported. A photochemical reduction of Ag^+ was applied and the deposition process was performed under UVA irradiation at room temperature for different periods of time. The TiO_2 anatase nanoplates were prepared using a solvothermal method. The molar ratio of Ag to the TiO_2 anatase nanoplates was 1:10. After the illumination the nanoplates appeared visually darker and silver nanoparticles were formatted on their surface. Their photocaralytic activity was tested in oxidizing NO gas to NO_2 and further to NO_3^-.

2. Experimental

The TiO_2 anatase nanoplates were fabricated *via* a solvothermal method. 3 mmol of titanium isopropoxide [$Ti(C_3H_7O)_4$] from Alfa Aesar Chemicals were dissolved into 50 mL of absolute ethanol

* Corresponding author. Tel.: +30 210 650 3343; fax: +30 210 651 9430.
E-mail address: trapalis@ims.demokritos.gr (C. Trapalis).

http://dx.doi.org/10.1016/j.apcatb.2014.02.030
0926-3373/

from Merck under vigorous stirring at room temperature. 0.6 mL of (0.03 mol) hydrofluoric acid (HF 40%) from Merck was added into the ethanol solution as a capping agent. Then the solution was poured into a 60 mL Teflon-lined autoclave and was subsequently placed into the oven for 24 h at 180 °C. In order to obtain fluoride free nanoplates, the collected reaction product was dispersed in 50 mL of 5 M NaOH aqueous solution and stirred for approximately 30 min. Then the dispersed product was centrifuged and washed several times until the pH value reached 7 and it was dried in a furnace at 70 °C overnight. In order to decorate the TiO_2 nanoplates with Ag nanoparticles on their {1 0 1} crystal facets a photodeposition procedure was performed as follows. The nanoplates were dispersed in methanol followed by the addition of $AgNO_3$ (5 mM). The obtained mixture was de-aerated with a flow of nitrogen gas and exposed to UVA light (365 nm) with a 10 W/m^2 irradiance at room temperature for 1, 5, 10 and 20 min respectively. The Ag decorated nanoplates were collected through centrifugation and washed several time with distilled water in order to remove any remaining unreacted $AgNO_3$ and finally dried in a furnace at 70 °C overnight.

The crystalline phase of the TiO_2 anatase nanoplates was investigated by X-ray diffractometry (SIEMENS D500 diffractometer) using CuK_α radiation. The measurements were performed using the following combination of slits: 1.0°/1.0°/1.0° as aperture diaphragms, 0.15° as detector diaphragm, and 0.15° as diffracted beam monochromator diaphragm. The measured 2θ range between 20° and 100° was scanned in steps of 0.03°/5 s. The accelerating voltage and applied current were 40 kV and 35 mA, correspondingly. The identification of the patterns was done with the cards of the International Centre for Diffraction Data. The shape and the crystal structure were observed with a transmission electron microscope (Philips CM20) operated at 200 kV and equipped with a Gatan GIF200 image filter. The TEM specimens of the Ag/TiO_2 anatase structures were prepared by direct deposition on a carbon coated Cu TEM grid. UV–vis diffuse reflectance spectra of all samples were obtained from the dry-pressed film samples using a UV–vis spectrometer (UV-2100, Shimadzu, Japan) with an integrating sphere attachment for the reflectance in the wavelength range of 200–900 nm. $BaSO_4$ was used as a reflectance standard. The absorbance spectra of the samples were calculated using the Kubelka–Munk phenomenological theory. The photoluminescence spectra were recorded through an automated imaging Spectrometer iHR320 (HORIBA JOBIN YVON) in conjunction with a He–Cd laser (Melles Griot Laser&Electro-optics Group) that works at 325 nm at room temperature.

The photocatalytic activity of the TiO_2 anatase nanoplates was studied in the oxidation of the NO gas following a modified ISO standard ISO/DIS 22197-1 [20]. The as-prepared samples were pressed in sample holders with an apparent surface area of 20 cm^2 (and not 100 cm^2 as mentioned in the ISO standard, as the amount of the samples produced was small) and then were pre-illuminated under a UVA lamp with a light irradiance of 10 W/m^2 for three days in order to remove all possible organic residual compounds from the sample's surfaces. After the pre-illumination period the sample holders containing the TiO_2 powders were placed into the flow-type photoreactor with their surface parallel to an optical quartz window and were illuminated by UVA radiation. The sample holders were separated from the window by a 5 mm thick air layer. The test gas passed only through the space between the sample holder and the window. The reactor is fabricated from materials that adsorb minimal NO and withstand irradiation of near-UV light. Before the reaction, the catalyst was exposed to the pollutant containing air stream with no illumination until dark adsorption equilibrium was reached. Afterwards the illumination was switched on. The Ag/TiO_2 anatase nanoplates were exposed to model air containing 1 ppm nitric oxide (NO). The photocatalyst adsorbs and oxidizes the NO to NO_2 and NO_3^- on its surface. The performance of the photocatalyst is determined by the amount of the net removal of the nitrogen oxide (NO). Pollutants and reaction products were analyzed *on-line*. For NO oxidation a nitrogen oxides (NO_x) APNA-370 HORIBA analyzer was used. The photocatalytic activity of the samples was evaluated under UVA light illumination with irradiance of 10 W/m^2 for 60 min. The photonic efficiency ζ (%) [21] of the TiO_2 anatase nanoplates for the NO oxidation was calculated using the following equation:

$$\zeta = \frac{n_{\text{degraded molecules}}}{n_{\text{available photons}}} = \frac{\int_{t_0}^{t_1} AX[\text{ppm}]dt}{q_{n,p}\Delta T} \times 100\% \quad (1)$$

where t_0 is the time moment when UVA light was switched on, t_1 is the time moment at the end of the illumination, T is determined by equation $\Delta T = t_1 - t_0$, A is the coefficient taken as a product of the gas flow value (3 L min^{-1}) and of the value 10^{-6} expressed in mol s^{-1} ($A = 2.08 \times 10^{-9}$ mol s^{-1}), X (taken in ppm) is either the difference between the initial NO/ NO_x concentration (~1 ppm) and the monitored NO/ NO_x concentration or the directly monitored NO_2 concentration. Lastly, $q_{n,p}$ is the photon flux of the samples' surface S (expressed in mol s^{-1}):

The photon flux [21] of the sample's surface (mol s^{-1}) can be calculated as follows:

$$q_{n,p} = \frac{E\lambda S}{N_A hc} \quad (2)$$

where E is the irradiance (W/m^2), S is the apparent surface area (m^2), λ is the wavelength (m), N_A is the Avogadro constant (mol^{-1}), h is Planck's constant (J s) and c is the speed of light (m/s).

The rate of the gas flow, with 50% relative humidity, into the flow-type photoreactor was 3 L min^{-1} for the NO gas. All samples were measured under identical conditions. The photonic efficiency of the monitored NO, NO_2, NO_x gases was calculated at the end of the illuminating period of time.

3. Results and discussion

Fig. 1 shows the XRD patterns of the pure and the Ag-decorated TiO_2 anatase nanoplates in different UVA illumination periods of time. It can be seen that the crystalline phase is anatase [JCPDS No. 021-1272 card] without any impurities of the remaining precursor that was used each time and/or the formation of another phase such as rutile or brookite. Certain Bragg peaks of the pure TiO_2 sample are broad due to the anisotropic growth of the nanoplates along the *c*-axis of the anatase lattice [22–24]. This indicates that the (0 0 1) surface of the TiO_2 anatase crystal is larger than the (1 0 1) surface. These observations are also present for the Ag-decorated TiO_2 samples which mean that their structure during the Ag photodeposition process is preserved. No diffraction peaks of metallic Ag were detected for the samples with short UVA illumination period of time due to their small size and high dispersion [25,27]. However, in the last sample with the largest UVA illumination period, diffraction peaks of metallic Ag particles [JCPDS No. 004-0783 card] were detected (Fig. 1(e_2)) as the nanoparticles became larger in size. Furthermore, the absence of oxidized forms such as Ag_2O or AgO in the XRD patterns suggests that Ag exists only in the metallic state in these samples.

As previously mentioned when the TiO_2 anatase nanoplates are band-gap illuminated electron and hole pairs are created which move to the surface of the nanoplates and are spatially separated. The electrons migrate to the {1 0 1} facets were as the holes migrate to the {0 0 1} facets. This means that the reduction reactions take place on the {1 0 1} facets where as the oxidation reactions take place on the {0 0 1} facets of the nanoplates [27]. In this present surface modification system, the surface electrons both act as reducing

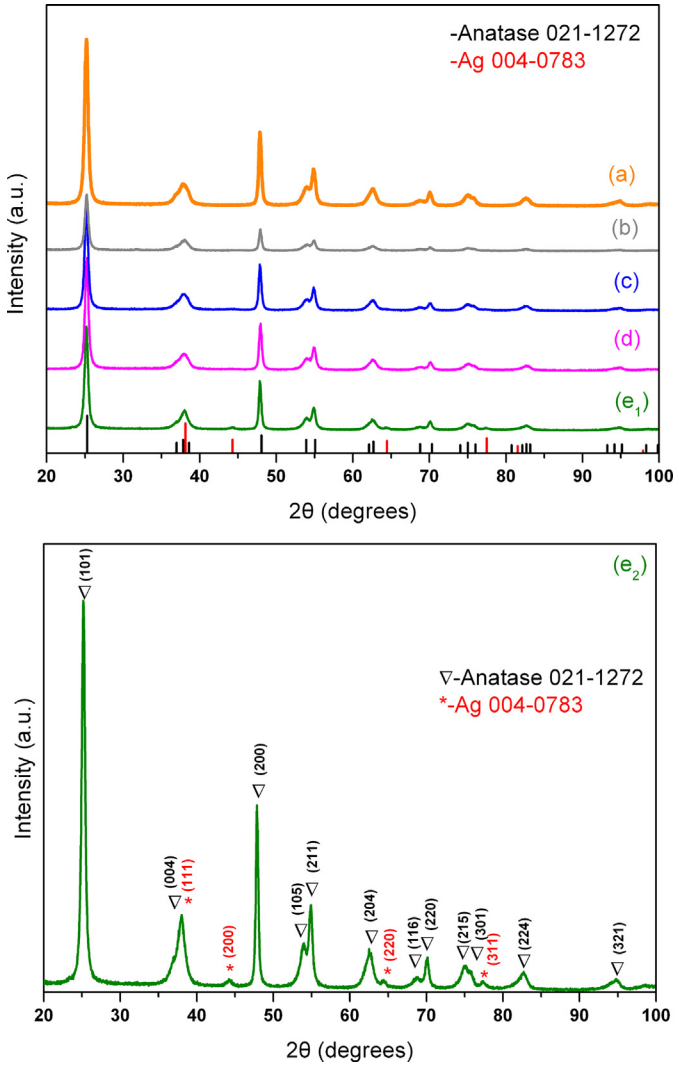

Fig. 1. XRD patterns of the pure (a) and Ag-decorated TiO_2 anatase nanoplates for different illumination periods (b) $t = 1$ min, (c) $t = 5$ min, (d) $t = 10$ min, (e) $t = 20$ min.

agents for the conversion of Ag^+ ions to metallic Ag and as negative charges for attracting Ag^+ to the {1 0 1} facets [28]. The holes on the other hand are consumed for the oxidation of methanol present in the system. Once the metallic Ag atoms are created, Ag clusters can be formed exclusively located on the {1 0 1} facets of the nanoplates, simply by aggregation of concurrently formed Ag atoms

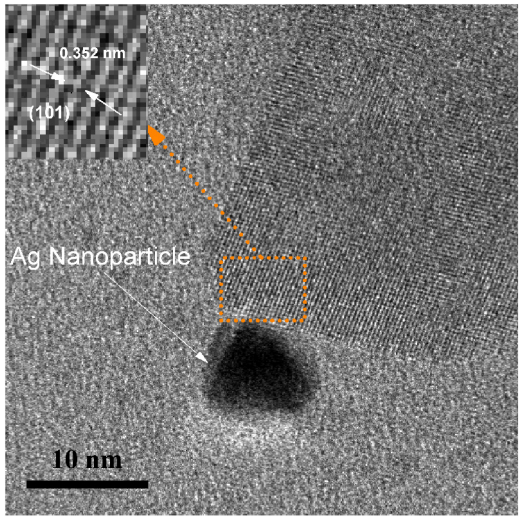

Fig. 2. TEM micrograph of an exclusively embedded Ag nanoparticle on the (1 0 1) surface of the nanoplate that corresponds to 10 min illumination period.

(Fig. 2). Furthermore, the presence of methanol adsorbed on the {0 0 1} facets of the nanoplates and its further oxidation from the surface localizes holes, hinders the migration of Ag atoms as well as the approach of Ag^+ ions on these particular surfaces. However, as the irradiation time was prolonged, together with the increase in Ag cluster size it was also observed a formation of some isolated Ag nanoparticles, which were consisted of smaller ones, and were detached from the surface of the nanoplates (Fig. 3(b)). For 1 min of irradiation the Ag nanoparticles are approximately 5 nm across (Fig. 3(a)). For 5, 10, 20 min of irradiation the Ag nanoparticles are 9, 16, 20 nm across respectively.

Fig. 4 shows the UV–vis absorbance spectra of the pure and the Ag-decorated TiO_2 anatase nanoplates. The absorbance spectra were calculated using the Kubelka–Munk method based on the diffuse reflectance spectra, where $F(R) = (1 - R)^2/2R$ [25]. As it can be seen, all samples absorb around 400 nm due to the band gap absorption of anatase TiO_2, which is ~3.2 eV. Also, the strong plasmon resonance absorption at wavelengths above 400 nm is caused by the Ag-decorated nanoparticles. Light absorbance by the photodeposited metal causes a collective oscillation of the free conduction band electrons of the silver nanoparticles as a consequence of their optical excitation. This phenomenon is observed when the wavelength of the incident light far exceeds the particle diameter. The absorption between 400 and 800 nm increases and a red shift is noticeable. This observation can be attributed to the

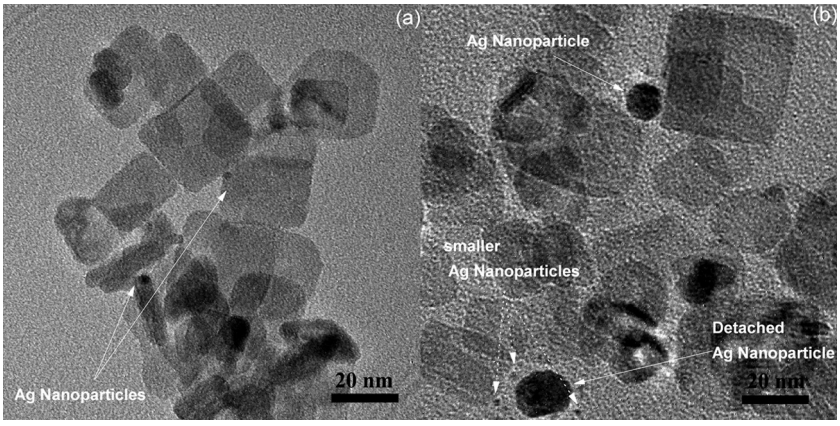

Fig. 3. TEM micrographs of the Ag-decorated TiO_2 anatase nanoplates for the shortest illumination period $t = 1$ min (b) and the longest $t = 20$ min.

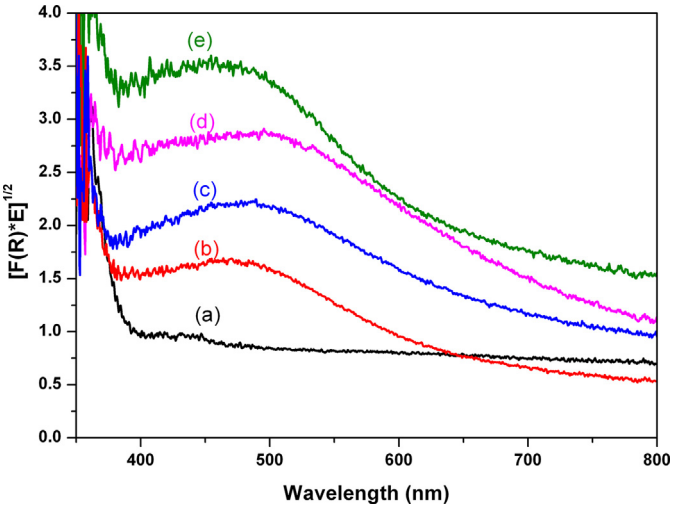

Fig. 4. Kubelka–Munk plot of the absorbance edge of the pure (a) and Ag-decorated TiO_2 anatase nanoplates for different illumination periods (b) $t = 1$ min, (c) $t = 5$ min, (d) $t = 10$ min, (e) $t = 20$ min.

size dependent surface plasmon resonance effect of metallic Ag. As the irradiation time is extended the size of the Ag nanoparticles increases. However, for the last sample (Fig. 4(e)) a small bleu shift is noticeable which is caused by the presence of smaller Ag nanoparticles in the sample. This observation comes also in agreement with the TEM micrograph that corresponds to this specific sample where big detached Ag nanoparticles and much smaller ones coexist (Fig. 2(b)).

Fig. 5 shows the photoluminescence spectra of the pure and Ag-decorated TiO_2 anatase nanoplates. One peak is observed for all samples at about 398 nm which is equivalent to 3.12 eV. One peak at about 513 nm which is equivalent to 2.42 eV is observed for the pure sample and for the two samples with short illumination periods (Fig. 5(a–c)). The photoluminescence peak at 398 nm is attributed to the emission of the band gap transition with the energy of the emitted light being equal to the band gap energy of anatase [29]. The other peak observed is caused by excitonic photoluminescence that results from surface oxygen vacancies and defects of the nanoplates [30,31]. The signal intensity of the pure anatase nanoplates is very strong and shows evident characteristics of the radiative recombination of the electrons and holes. More specifically, the photoluminescence intensities of the samples decrease,

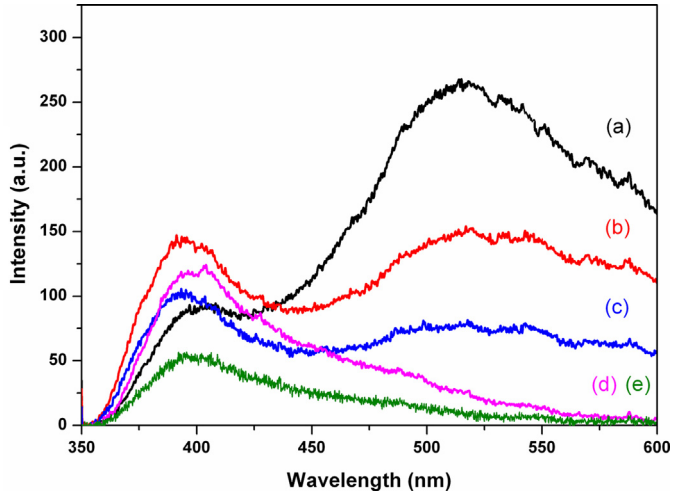

Fig. 5. PL spectra of the pure (a) and Ag-decorated TiO_2 anatase nanoplates for different illumination periods (b) $t = 1$ min, (c) $t = 5$ min, (d) $t = 10$ min, (e) $t = 20$ min.

according to the size of the silver decorated nanoparticles on the nanoplates. It is known that the photoluminescence intensity of the Ag-decorated TiO_2 anatase nanoplates is affected by two factors. The first factor is the migration of the electrons from the nanoplates to the Ag nanoparticles and the second is the Ag plasmon absorption [32]. Ag deposition favours the transfer of photo-induced electrons and holes by forming a Schottky barrier at the metal-semiconductor interface [33]. Therefore the Ag-decorated nanoplates have lower intensities than the pure anatase nanoplates which are indicating of a lower recombination rate. Consequently, the recombination of the charge carriers is effectively suppressed by the Ag photodeposition on the surface.

The photocatalytic activity of the pure and the Ag-decorated TiO_2 anatase nanoplates was evaluated by oxidizing NO gas. In principle the photocatalyst is activated by light, in the case of TiO_2 by UVA irradiation, forming this way an electron and hole pair (e^-/h^+):

$$\text{Ag-decorated } TiO_2 + h\nu \rightarrow h^+ + e^- \quad (3)$$

The electron migrates first to the {1 0 1} crystal facets of the TiO_2 anatase nanoplates [12,13] and then passes on to the Ag decorated nanoparticles on these specific facets and finally reacts with the favourably adsorbed O_2 molecules on the Ag nanoparticles [34] forming superoxide anions (O_2^-):

$$e^- + O_2 \rightarrow O_2^- \quad (4)$$

The superoxide anion O_2^- is a base and will form HO_2 radicals with traces of water that is originated from the humidity of the air flow [35–38]. The HO_2 may recombine to give H_2O_2:

$$2HO_2 \rightarrow H_2O_2 + O_2 \quad (5)$$

or may react with the NO gas, which is adsorbed on the {1 0 1} crystal facets of the TiO_2 anatase nanoplates, forming NO_2 and a hydroxyl radical [39]:

$$HO_2 + NO \rightarrow NO_2 + OH \quad (6)$$

The products from the above reaction can further react to the end product which is nitric acid (HNO_3):

$$NO_2 + OH \rightarrow HNO_3 \quad (7)$$

All nitrogen species (NO, NO_2) are photocatalytically oxidized leading to nitrate (NO_3^-) whereas O_2 is photochemically reduced.

The photogenerated holes that migrate to the {0 0 1} crystal facets of the TiO_2 anatase nanopaltes react with the dissociated water molecules that are present on these particular facets creating active oxygen species [39,40]:

$$H_2O + h^+ \rightarrow H^+ + OH \quad (8)$$

Previous experimental studies have shown that no photocatalytic decomposition of the NO gas was observed in the absence of O_2, since no HO_2 was formed in nitrogen gas and also the photogenerated holes that migrate to the {0 0 1} facets of the anatase crystal do not take part in the oxidation of the NO gas [41,42]. Furthermore, it was shown that the first order rate constants for photochemical reactions of NO and NO_2 with TiO_2 are independent of the type of mixture of nitrogen oxides. This means that there is no inhibition of the decomposition of one compound by the other under the experimental conditions applied [41]. Fig. 6 shows the photonic efficiencies of NO, NO_2 and NO_x gases for the pure and the Ag-decorated TiO_2 anatase nanoplates. It is obvious that the photocatalytic activity of the Ag-decorated nanoplates has been enhanced. More specifically, they exhibited a lower photonic efficiency for NO_2 production and a higher one for NO oxidation in comparison to the pure anatase nanoplates, which means that a large amount of the NO gas was oxidized to nitrate (NO_3^-) and only a small amount of NO_2 gas was produced. The silver nanoparticles

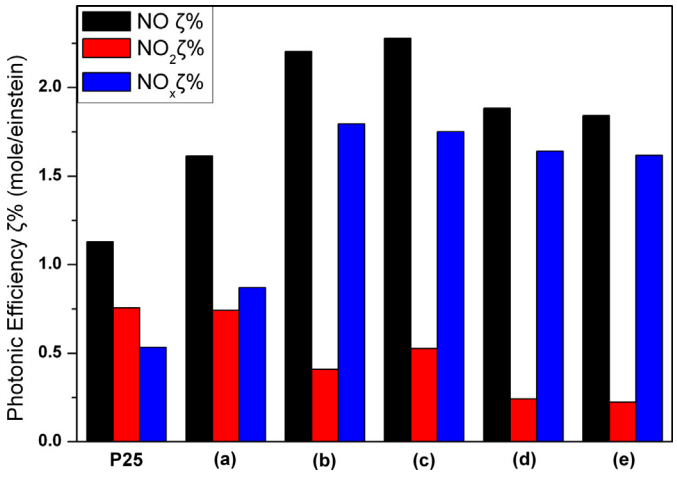

Fig. 6. Photonic efficiency for NO oxidation of the pure (a) and Ag-decorated TiO_2 anatase nanoplates for different illumination periods (b) $t = 1$ min, (c) $t = 5$ min, (d) $t = 10$ min, (e) $t = 20$ min.

on the surface of the nanoplates created a Schottky barrier. The photogenerated electrons where stored by the Ag, which facilitates the charge separation in the semiconductor-metal composite system [32,43,44]. Consequently, the Ag-decorated nanoplates exhibited enhanced photocatalytic activity and higher photonic efficiencies in comparison to the pure TiO_2 nanoplates. Certainly, there is an optimum size for the Ag nanoparticles. As their size becomes larger, they may cover active sites on the TiO_2 surface and also affect the electron storage capacity [32]. Therefore their photocatalytic activity is slightly reduced but still enhanced compared to the pure TiO_2 anatase nanoplates. More specifically, it can be seen in Figure 6(c) that the optimum size for the Ag nanoparticles on the {1 0 1} crystal facet of the TiO_2 anatase nanoplates is 9 nm. In this size the nanoparticles do not block any of the active sites of the photocatalyst, as this sample performed the best photocatalytic behaviour. Apparently a high concentration of TiO_2 e^-/h^+ pairs were yielded in this sample, leading to a very high photochemical oxidation of the NO forming nitrate as a final product while O_2 is photochemically reduced.

4. Conclusions

TiO_2 anatase nanoplates were fabricated by combining a solvothermal method and hydrofluoric acid as a capping agent in order to fabricate pure and well defined anatase nanoplates with exposed {0 0 1} crystal facets. The removal of the adsorbed fluoride atoms was accomplished by washing them with a NaOH aqueous solution. The decoration with Ag nanoparticles on the {1 0 1} crystal facets of the nanoplates was achieved by using degassed methanol as a hole scavenger while the Ag^+ ions in the methanol solution were photoreduced by the migrated e^- on the (1 0 1) surfaces in the presence of UVA irradiation. The size of the Ag nanoparticles was controlled by varying the illumination period of time. The XRD diffraction peaks of all samples showed the same anisotropic broadening along the c-axis of the anatase lattice. This indicates that the structure of the nanoplates during the Ag photodeposition process was preserved. Moreover, plasmon resonance absorption at wavelengths above 400 nm is caused by the Ag-decorated nanoparticles and increases with the increase of the Ag content. The PL signal of the pure TiO_2 sample is very strong showing evident characteristics of the recombination of the electrons and holes. All Ag-decorated TiO_2 nanoplates exhibited enhanced photocatalytic properties in comparison to the pure TiO_2 nanoplates due to the lower recombination rate of the photogenerated electrons and holes. The sample that exhibited the best photocatalytic activity and the highest photonic efficiency was the one that had 9 nm size Ag-decorated nanoparticles.

Acknowledgements

This work was supported by the General Secretary of Research and Technology of Greece (09SYN-42-925). The authors would like also to thank Prof. D. Bahnemann and Dr. R. Dillert from the Institut fuer Technische Chemie, Leibniz Universitaet Hannover, Germany, for the fruitful discussion on the NO oxidation during the program for promotion of the exchange and scientific cooperation between Greece and Germany (IKYDA 2009).

References

[1] J. Sunyer, Eur. Respir. J. 5 (2001) 1024–1033.
[2] C. Goss, S. Newsom, J. Schildcrout, L. Sheppard, J.D. Kaufman, Am. J. Respir. Crit. Care. Med. 7 (2004) 816–821.
[3] A. Fujishima, K. Honda, Nature 238 (1972) 37–38.
[4] M.R. Hoffmann, S.T. Martin, W. Choi, D.W. Bahnemann, Chem. Rev. 95 (1995) 69–96.
[5] K.L. Lv, B. Cheng, J.G. Yu, G. Liu, Phys. Chem. Chem. Phys. 14 (2012) 5349–5362.
[6] Q.J. Xiang, J.G. Yu, Chinese J. Catal. 32 (2011) 525–531.
[7] K.L. Lv, Q.J. Xiang, J.G. Yu, Appl. Catal., B 104 (2011) 275–281.
[8] Q.J. Xiang, K.L. Lv, J.G. Yu, Appl. Catal., B 96 (2010) 557–564.
[9] J.G. Yu, J.J. Fan, K.L. Lv, Nanoscale 2 (2010) 2144–2149.
[10] A. Fujishima, X. Zhang, D.A. Tryk, Surf. Sci. Rep. 63 (2008) 515–582.
[11] X.Q. Gong, A. Selloni, J. Phys. Chem. B 109 (2005) 19560–19562.
[12] T. Ohno, K. Sarukawa, M. Matsumura, New J. Chem. 26 (2002) 1167–1170.
[13] W.Q. Fang, X.Q. Gong, H.G. Yang, J. Phys. Chem. Lett. 2 (2011) 725–734.
[14] T. Tachikawa, S. Yamashita, T. Majima, J. Am. Chem. Soc, 133 (2011) 7197–7204.
[15] S. Ko, C.B. Banerjee, J. Sankar, Composites Part B 42 (2011) 579–583.
[16] L. Lu, S. Hu, H.I. Lee, C. Wo, R.A. Fischer, J. Nanopart. Res. 9 (2007) 491.
[17] H. Tada, T. Ishida, A. Takao, S. Ito, Langmuir 20 (2004) 7898–7900.
[18] C. Hu, Y.Q. Lan, J.H. Qu, X.X. Hu, A. Wang, J. Phys. Chem. B 110 (2006) 4066–4072.
[19] W. Grünert, A. Brückner, H. Hofmeister, P. Claus, J. Phys. Chem. B 108 (2004) 5709–5717.
[20] ISO/DIS 22197-1 Fine ceramics (advanced ceramics, advanced technical ceramics). Test method for air-purification performance of semiconducting photocatalytic materials. Part 1. Removal of nitric oxide.
[21] M.V. Sofianou, C. Trapalis, V. Psycharis, N. Boukos, T. Vaimakis, J.G. Yu, W.G. Wang, Environ. Sci. Pollut. Res. 19 (2012) 3719–3726.
[22] C. Greaves, J. Appl. Cryst. 18 (1985) 48–50.
[23] J.I. Langford, D. Louër, J. Appl. Cryst. 15 (1982) 20–26.
[24] Th.E. Weirich, M. Winterer, S. Seifried, H. Hahn, H. Fuess, Ultramicroscopy 81 (2000) 263–270.
[25] L.P. Wen, B.S. Liu, C. Liu, X.J. Zhao, J. Wuhan Univ. 24 (2008) 258–263.
[27] H.H. Mohamed, R. Dillert, D.W. Bahnemann, Chem A: Europ. J. 18 (2012) 4314–4321.
[28] C.T. Dinh, T.D. Nguyen, F. Kleitz, T.O. Do, ACS Appl. Mater. Interfaces 3 (2011) 2228–2234.
[29] J.G. Yu, Q.J. Xiang, J.R. Ran, S. Mann, CrystEngComm. 12 (2010) 872–879.
[30] J.G. Yu, L.F. Qi, M. Jaroniec, J. Phys. Chem. C 114 (2010) 13118–13125.
[31] J.G. Yu, H.T. Guo, S.A. Davis, S. Mann, Adv. Funct. Mater. 16 (2006) 2035.
[32] A. Takai, P.V. Kamat, ACS Nano 5 (2011) 7369–7376.
[33] A.L. Linsebigler, G. Lu, J.T. Yates Jr., Chem. Rev. 95 (1995) 735–758.
[34] R. Wanbayor, V. Ruangpornvisuti, J. Mol. Struct. THEOCHEM 952 (2010) 103–108.
[35] C. Kormann, D.W. Bahnemann, M.R. Hoffmann, Environ. Sci. Technol. 22 (1988) 798–806.
[36] W. Kubo, T. Tatsuma, Anal. Sci. 20 (2004) 591–593.
[37] T. Hirakawal, Y. Nosaha, J. Phys. Chem. C 112 (2008) 15818–15823.
[38] K. Hashimoto, K. Wasada, N. Toukai, H. Kominami, Y. Kera, J. Photochem. Photobiol. A: Chem. 136 (2000) 103–109.
[39] H. Einaga, A. Ogata, J. Hazard. Mater. 164 (2009) 1236–1241.
[40] S. Matsuda, H. Hatano, Powder Technol. 151 (2005) 61–67.
[41] S. Laufs, G. Burgeth, W. Duttlinger, R. Kurtenbach, M. Maban, C. Thomas, P. Wiesen, J. Kleffmann, Atmos. Environ. 44 (2010) 2341–2349.
[42] M.V. Sofianou, V. Psycharis, N. Boukos, T. Vaimakis, J.G. Yu, R. Dillert, D. Banhemann, C. Trapali, Appl. Catal., B 142-143 (2013) 761–768.
[43] J.G. Yu, J.F. Xiong, B. Cheng, S.W. Liu, Appl. Catal., B 60 (2005) 211–221.
[44] W.G. Wang, J.G. Yu, Q.J. Yu, Q.J. Xiang, B. Cheng, Appl. Catal., B 119-120 (2012) 109–116.